ISSN 0036-0244, Russian Journal of Physical Chemistry A, 2018, Vol. 92, No. 3, pp. 456–465. © Pleiades Publishing, Ltd., 2018.

CHEMICAL KINETICS AND CATALYSIS

Ordered Mesoporous NiCeAl Containing Catalysts for Hydrogenolysis of Sorbitol to Glycols[1]

Zhiwei Zhou[a], Jiaqi Zhang[a], Juan Qin[b], Dong Li[a], and Wenliang Wu[a,*]

[a] *College of Chemical Engineering, Nanjing Tech University, Nanjing, 210009 China*

[b] *Technology and Finance Service Center of Jiangsu Province, Productivity Center of Jiangsu Province, Nanjing, 210042 China*

**e-mail: wwl@njtech.edu.cn*

Received November 1, 2016

Abstract—Cellulose-derived sorbitol is emerging as a feasible and renewable feedstock for the production of value-added chemicals. Highly active and stable catalyst is essential for sorbitol hydrogenolysis. Ordered mesoporous M–*x*Ni*y*CeAl catalysts with different loadings of nickel and cerium species were successfully synthesized via one-pot evaporation-induced self-assembly strategy (EISA) and their catalytic performance were tested in the hydrogenolysis of sorbitol. The physical chemical properties for the catalysts were characterized by XRD, N_2 physisorption, H_2-TPR, H_2 impulse chemisorption, ICP and TEM techniques. The results showed that the ordered mesopores with uniform pore sizes can be obtained and the Ni nanoparticles around 6 nm in size were homogeneously dispersed in the mesopore channels. A little amount of cerium species introduced would be beneficial to their textural properties resulting in higher Ni dispersion, metal area and smaller size of Ni nanoparticles. The M–10Ni2CeAl catalyst with Ni and Ce loading of 10.9 and 6.3 wt % shows better catalytic performance than other catalysts, and the yield of 1,2-PG and EG can reach 56.9% at 493 K and 6 MPa pressure for 8 h after repeating reactions for 12 times without obvious deterioration of physical and chemical properties. Ordered mesoporous M–NiCeAl catalysts are active and stable in sorbitol hydrogenolysis.

Keywords: sorbitol, hydrogenolysis, NiCeAl, EISA, mesoporous

DOI: 10.1134/S0036024418030378

INTRODUCTION

Nowadays, increasing environmental concerns have spurred extensive investigation into utilization of biomass [1–5]. Sorbitol is one of the twelve building blocks derived from biomass, and it can be produced from renewable cellulose by hydrolysis followed by hydrogenation [6–8]. The catalytic hydrogenolysis of sorbitol to value-added chemicals such as ethylene glycol (EG) and propylene glycol (PG) has been extensively investigated in the recent decades [9–11].

According to the mechanism for hydrogenolysis of polyol proposed by Wang et al. [12] polyol is firstly dehydrogenated to form β-hydroxyl carbonyl on metal active sites, especially some transition metal catalysts, such as Ru, Pt, and Ni, and then undergoes C–C bond cleavage through retro-aldol strategy and C–O bond cleavage by dehydration. Zhao et al. reported that carbon nanofiber was more suitable for supporting Ru catalysts than activated carbon and showed higher sorbitol conversion and EG and PG selectivity, the catalytic performance would be promoted by introduction of small amount of alkaline substances [13]. Wang et al. found that Ni–MgO catalysts showed higher catalytic performance in the hydrogenolysis of sorbitol for preparation of glycerol and glycols than Co–MgO and Cu–MgO catalysts [14]. The reason for the differences can be ascribed to their distinct dehydrogenation/hydrogenation activities. Similarly, the Ni–NaY catalysts was more active in hydrogenolysis of sorbitol than Ru–NaY and Pt–NaY catalysts [15]. Therefore, Ni-based catalysts, which are cheaper than noble metals such as Ru and Pt and show good catalytic performance for C–C cleavage reaction, could be regarded as potential catalysts for industrial applications. However, it is still a challenge to prepare highly active and stable Ni-based catalysts.

It has been demonstrated that preparation method and catalyst support have significant impact on the dispersion of Ni species, which would further significantly affect the catalytic performance and stability [16, 17]. Many carriers including metal oxide [18], zeolite [19] and some methods such as co-precipitation, impregnation and decomposition have been adopted for elevating the physical and chemical properties and catalytic performance of Ni-based catalysts [20]. However, agglomeration of Ni nanoparticles was observed resulting in gradual deactivation of the catalysts. It is important and crucial to carefully design and

[1] The article is published in the original.

control the physical composition and preparation process of the catalyst to improve its catalytic activity and stability.

Confining or embedding Ni nanoparticles in hydrothermally stable porous supports are alternative methods to control its particle size because it can prohibit the agglomeration of Ni nanoparticles. Compared to the catalysts prepared by conventional impregnation or coprecipitation methods, ordered mesoporous alumina supported Ni nanoparticles with superior textural properties and thermal stability by one-pot evaporation induced self-assembly (EISA) method can be obtained, which is owing to the reason that nickel species would be reduced and embedded in the wall of mesoporous alumina resulting in smaller size of Ni nanoparticles and their more homogeneous dispersion. At the same time, the introduction of small amounts of rare earth into the sol-gel process could rationally restrain the crystal growth of nickel species and its size would be effectively controlled during the following calcination process with high temperature, and the obtained samples with relatively large specific surface area, uniform mesopore channels and large pore volume show excellent catalytic performance in the methane dry reforming [21–24]. Therefore, the Ni–CeO_2–Al_2O_3 catalysts prepared via EISA method should have promising catalytic performance in the hydrogenolysis of sorbitol. However, to the best of our knowledge, there is no report in the literature for the hydrogenolysis of sorbitol on these catalysts.

In this paper, a series of Ni–CeO_2–Al_2O_3 catalysts with ordered mesoporous structures were successfully synthesized in a one-pot EISA procedure. The textural and physical chemical properties of the catalysts were carefully characterized and their catalytic activity, selectivity and stability in the hydrogenolysis of sorbitol were also investigated.

EXPERIMENTAL

Catalyst Preparation

$(EO)_{20}(PO)_{70}(EO)_{20}$ triblock copolymer (Pluronic P123, typical M_n = 5800, Sigma-Aldrich), nitric acid (HNO_3, Baiyin Liangyou Chemical Reagent Co. Ltd.), aluminum isopropoxide ($C_9H_{21}AlO_3$, Sigma-Aldrich), nickel nitrate hexahydrate ($Ni(NO_3)_2 \cdot 6H_2O$, Shanghai NO.2 Reagent Factory, China), cerium nitrate hexahydrate ($Ce(NO_3)_3 \cdot 6H_2O$, Shanghai Shanpu Chemical Co. Ltd., China) and anhydrous ethanol (C_2H_5OH, Sinopharm Chemical Reagent Co. Ltd.) employed in this study were all A.R. grade. All the chemicals were used as received without further purification.

Ordered mesoporous Ni–CeO_2–Al_2O_3 samples were synthesized *via* improved one-pot EISA strategy based on previously reported in the literature [21]. In a typical procedure, 1.0 g of P123 was dissolved with 20 mL of C_2H_5OH at 313 K, and then 1.6 mL of HNO_3 and A mmol of $C_9H_{21}AlO_3$ were added. After stirring for 30 min, B mmol $Ni(NO_3)_2 \cdot 6H_2O$ and C mmol $Ce(NO_3)_3 \cdot 6H_2O$ ($A + B + C = 10$ mmol) were introduced into the above solution. The mixture was stirred at 313 K in a beaker covered with PE film for another 6 h and then transferred to a Petri dish for evaporation at 333 K for 96 h to fully evaporate the ethanol. The as-prepared gel was calcined at 873 K for 6 h in air with a ramping rate of 1.5 K/min to obtain mesoporous NiO–CeO_2–Al_2O_3 oxides. Then NiO–CeO_2–Al_2O_3 samples were reduced in H_2 flow at 1073 K for 2 h with a ramping rate of 1.5 K/min to prepare Ni–CeO_2–Al_2O_3 catalysts and denoted as M–*x*Ni*y*CeAl, where *x* and *y* stand for the molar percent of nickel species and cerium species, respectively. Ordered mesoporous Al_2O_3, CeO_2–Al_2O_3 and Ni–Al_2O_3 were also prepared in the same strategy and named as M–Al_2O_3, M–*y*CeAl, and M–*x*NiAl.

Characterization Techniques

XRD patterns of the samples were obtained on a Bruker D8 instrument with Ni-filtered CuK_α radiation ($\lambda = 0.1538$ nm) and operated at 30 mA and 40 kV. The scanning angle was in the 2θ ranges from 0.5° to 8° (Low-angle XRD, LXRD) and from 10° to 80° (Wide-angle XRD, WXRD). The nitrogen physisorption isotherms and pore size distribution were measured at 77 K by using a BELSORP-MINI analyzer with the samples being degassed at 573 K for 3 h before analysis. The surface area was calculated by Brunauer–Emmett–Teller (BET) method, and the pore size distribution was obtained by using the Barrett–Joyner–Halenda (BJH) adsorption model. H_2-TPR analysis was carried out over Micromeritics Autochem II 2920. The samples were pretreated in the Ar stream at 623 K for 2 h. The reduction temperature was raised from 323 to 1273 K at a rate of 10 K min^{-1} in 10% H_2/Ar flow (30 mL/min). Ni dispersion and Ni metallic surface area were calculated through H_2 pulse chemisorption test over Micromeritics Autochem II 2920 instrument automatically. The as-reduced catalysts were pretreated in Ar flow at 773 K for 2 h and then were cooled down to 323 K in Ar flow. H_2 pulse chemisorption test was carried out by pulsing a mixture of 10% H_2/Ar (30 mL/min). The nickel surface areas were calculated from the volume of H_2 adsorbed assuming the stoichiometric ratio $H_{adsorbed}/Ni_{surface} = 1$ and that a density of active sites on the surface of 1.54×10^{19} Ni atoms/m^2. The metal compositions of the catalysts were analyzed by inductively coupled plasma atomic emission spectroscopy (ICP-AES) on a Perkin-Elmer optima 2100 DV device. TEM analysis was performed on a JEM-2100 (JEOL) electron microscope operating at 200 kV.

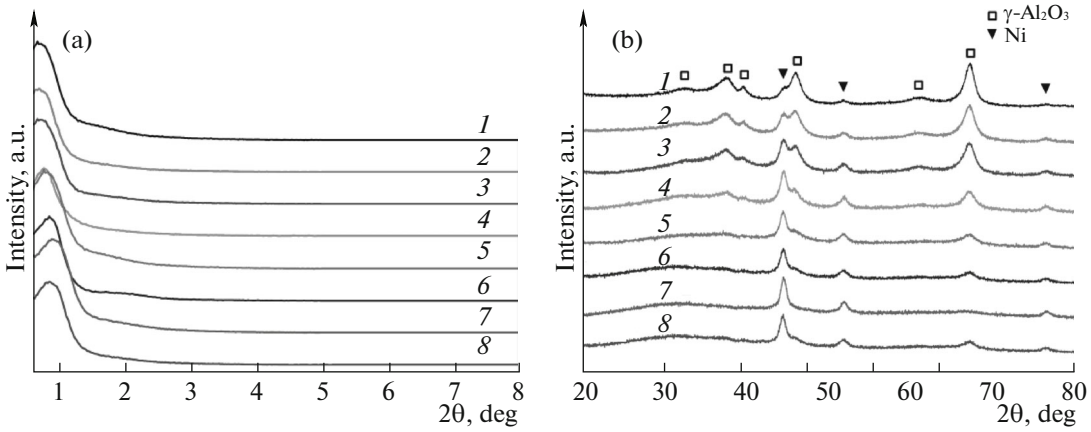

Fig. 1. Low-angle (a) and wide-angle (b) XRD patterns of as-reduced catalysts; (*1*–*7*) M–*x*Ni*y*CeAl, (*8*) M–10Ni$_2$CeAl–RT; $x = 4$ (*1*), 6 (*2*), 8 (*3*), 10 (*4*–*7*), $y = 0$ (*1*–*4*), 1 (*5*), 2 (*6*), 4 (*7*).

Catalytic Performance Test

Hydrogenolysis of sorbitol was carried out in a 100 mL stainless steel autoclave equipped with a mechanical stirrer. In a typical experiment, 20 mL of 30 wt % sorbitol aqueous solution, 0.6 g of catalyst, and 0.1 g of $Ca(OH)_2$ were placed into the reactor. The autoclave was sealed, purged with H_2 for three times, heated up to desired temperature and pressurized to desired pressure, and subsequently stirred at a rate of 500 rpm. After the reaction, the reactor was cooled to room temperature and decompressed. The gas phase products were detected on gas chromatograph (Agilent 7890A) equipped with a TDX-01 packed column and thermal conductivity detector (TCD). The liquid phase products were detected by HPLC (Thermo Fisher Ultimate 3000, redistilled water as flowing phase) equipped with a Hyper REZ XP Carbohydrate Ca^{2+} 8 μm column and a refractive index detector (RID). The major products were 1,2-PG, EG, and glycerol. Small amounts of other by-products, namely xylitol, erythritol, butanediol, lactic acid, ethanol, methanol, CH_4 and CO_2 were also detected. The products were verified using authentic samples and quantified by an external standard method. Carbon balance (CB) measurements including the detected organic and inorganic carbons for all the experiments were all over 90%. In this work, the glycols refer to the sum of EG and 1,2-PG. In the recycling process, the catalyst was separated with centrifugation followed by washing with ethanol for three times and dried without further treatment.

$$\text{Sorbitol selectivity} = \frac{(\text{initial mmol of sorbitol}) - (\text{mmol of sorbitol left})}{\text{initial mmol of sorbitol}} \times 100\%,$$

$$\text{Product selectivity} = \frac{(\text{mmol of product}) \times (\text{number of carbon atoms in product})}{((\text{initial mmol of sorbitol}) - (\text{mmol of sorbitol left})) \times 6} \times 100\%,$$

$$\text{Yield of glycols} = \text{Sorbitol conversion} \times (\text{EG selectivity} + \text{1,2-PG selectivity}) \times 100\%.$$

RESULTS AND DISCUSSION

Catalyst Characterization Results

LXRD patterns of different catalysts were displayed in Fig. 1a. All the as-reduced catalysts showed strong diffraction peaks centered at around 0.6°–0.9°, together with weak peaks around 1.5°, suggesting the successful formation of ordered mesoporous structure. The ordered mesoporous frameworks were preserved after calcination at 873 K and reduction at 1073 K, showing the excellent thermal stability of mesoporous structure. The incorporation of Ni and Ce species did not significantly affect the mesoporous structure of the samples.

Figure 1b presented the WXRD patterns of these catalysts. Weak diffraction peaks owing to the low crystallinity centered at 31.9°, 37.6°, 39.5°, 45.9°, 60.9°, and 66.9° ascribing to γ-Al_2O_3 crystal can be observed for all the catalysts, and the intensities of these peaks decreased with the nickel species loading increasing. In addition, diffraction peaks centered at 44.5°, 51.8°, and 76.4° assigned to metallic Ni (JCPDS card no. 87-0712) can be found, and these peaks were relatively broad, implying the well disper-

Table 1. Physical properties of as-reduced catalysts

Sample	S_{BET}, $m^2 g^{-1}$	V, $cm^3 g^{-1}$	d, nm	D, %	s, $m^2 g^{-1}$ cat.	d_{Ni} ±0.2 nm	Ni, wt %	Ce, wt %
M-4NiAl	202	0.48	9.2	8.2	1.2	–	4.7	0
M-6NiAl	186	0.43	9.4	7.1	1.7	5.1	6.6	0
M-8NiAl	179	0.42	9.4	5.9	2.0	6.2	9.1	0
M-10NiAl	173	0.41	9.6	5.1	2.2	7.1	11.4	0
M-10Ni1CeAl	196	0.44	9.8	5.7	2.4	6.3	11.1	3.2
M-10Ni2CeAl	191	0.44	10.1	6.3	2.6	6.1	10.9	6.3
M-10Ni4CeAl	184	0.43	10.6	6.4	2.7	6.5	10.2	12.1
M-10Ni2CeAl-RT	177	0.42	10.3	6.2	2.5	6.7	10.8	6.3

d_{Ni} is particle size, V is total pore volume, d is average pore diameter, D is dispersion, s is metal area.

sion and small particle size of Ni nanoparticles. Average particle sizes of metallic Ni nanoparticles in the range of 5.1–7.1 nm seen in Table 1 were calculated by Scherrer equation based on diffraction peaks at 51.8° of Ni (200) plane. The low XRD reflections of metallic Ni may lead to a little inaccuracy in the determination of crystalline sizes. Nevertheless, quantitative estimation of crystallite sizes with Scherrer equation could provide useful information for comparative purposes. No diffraction peaks corresponding to cerium species for all the catalysts, illustrating their well dispersion. The weight contents of Ni and Ce elements in the samples were determined by ICP and listed in Table 1.

Nitrogen physisorption analysis could provide information about textural properties of porous materials. Nitrogen adsorption-desorption isotherms and pore size distributions were displayed in Fig. 2. As shown in Fig. 2a, all the M–*x*Ni*y*CeAl catalysts possessed type IV isotherms with H1 shaped hysteresis loops, which were significant features of ordered mesoporous materials with cylindrically shaped channels. The pore size distributions of the catalysts exhibited in Fig. 2b were narrow, confirming the uniformity of the mesopores.

Textural properties of the as-reduced M–*x*Ni*y*-CeAl catalysts were summarized in Table 1. It could be observed that all the samples possessed relatively large specific surface areas (173–202 m^2/g), which was beneficial to provide enough surface area for the dispersion of Ni nanoparticles. Big pore volumes up to 0.48 cm^3/g and average pore size in the range of 9.2–10.6 nm for these samples were obtained, which would beneficial to diffusion of reactants and products, especially relatively large molecule substrates. In addition, Ni nanoparticle sizes were located in the range of 5.1–7.1 nm with Ni weight loading up to 11.4%, which were relatively small for Ni-based catalysts and smaller than the average pore sizes of the catalysts, suggesting that the Ni nanoparticles can be dispersed in the internal mesopore channels and would not lead to blocking of the mesopores. Compared with M–10NiAl catalyst, the surface areas and pore volumes for M–10Ni*y*CeAl samples by introduction of little cerium species were promoted, which resulted in higher Ni dispersion and metal area and smaller size of Ni nanoparticles, which should be beneficial to the catalytic performance in the hydrogenolysis of sorbitol.

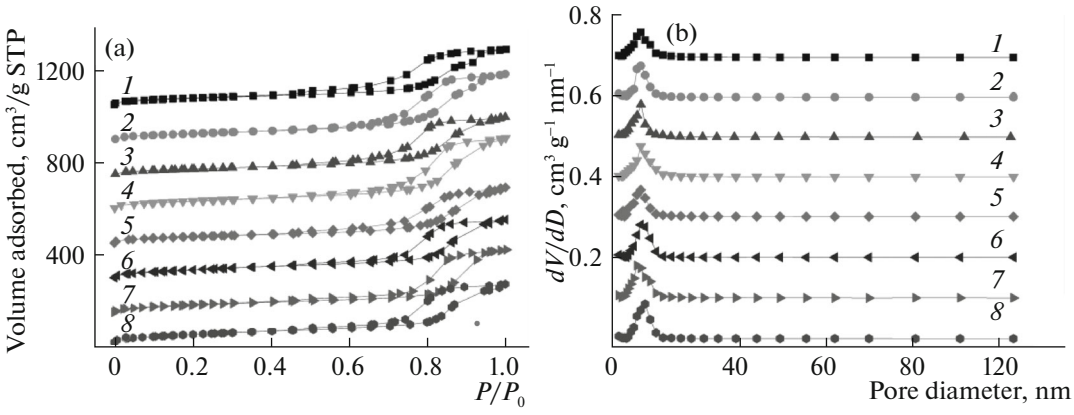

Fig. 2. (a) N_2 adsorption-desorption isotherms and (b) pore size distributions for as-reduced catalysts; notes see Fig. 1.

H_2-TPR technique is an effective method for determining the reducibility of the catalysts, which could provide information about the interaction between the active metal species and their supports. H_2-TPR profiles of the as-calcined samples were shown in Fig. 3. All the samples prepared with EISA process exhibited similar profiles of hydrogen reduction, showing only one obvious reduction peak in the range from 800 to 1100 K, regardless of the contents of nickel and cerium species. No evident reduction peak in the range of 623–723 K corresponding to dissociated or free NiO was observed, implying that the strong interaction between Ni nanoparticles and the ordered mesoporous framework were formed. It can be seen that the locations of peaks gradually migrated toward lower temperatures at higher Ni contents, suggesting the formation of weaker interaction. Compared to the M–10NiAl sample, reduction temperature of M–10Ni*y*CeAl catalysts were lower, and the peaks gradually migrated to lower temperatures with the increase of Ce contents, indicating that the introduction of little Ce species would promote reduction of Ni species, which was consistent with previous reports [25].

Impulse chemisorption of H_2 at 298 K was used to determine the nickel dispersion and metallic Ni surface area on the surface of the support, and the results for M–*x*Ni*y*CeAl catalysts were given in Table 1. With the increase of Ni content, metal area of nickel per gram of catalyst increased, while its dispersion decreased gradually owing to the bigger size of Ni nanoparticles probably. However, it was evidently found that both the dispersion and metal area of Ni nanoparticles were improved after introduction of little cerium, suggesting that the incorporation of cerium species was beneficial to the dispersion of Ni nanoparticles resulting in their smaller sizes.

Hydrogenolysis of Sorbitol

Hydrogenolysis of sorbitol over different catalysts was carried out and the results were listed in Table 2. It could be seen that no sorbitol could be transformed in the absence of catalyst or when the M–Al_2O_3 or M–2CeAl was added. However, it was notable to find that many products can be obtained over the M–Ni*y*CeAl catalysts, where the main products were glycerol, 1,2-PG and EG. Other products such as erythritol, 1,2-butanediol, xylitol, lactic acid, ethanol, methanol, 1-propanol, 2-propanol and gaseous products of CH_4 and CO_2 were also detected. On the basis of the results above, it could be concluded that the Ni nanoparticles were active catalytic sites and were essential for the hydrogenolysis of sorbitol.

Sorbitol conversion was promoted with increasing Ni nanoparticle loadings, and sorbitol conversion reached up to 40.8% over the M–10NiAl catalyst. Compared to the results of M–10NiAl catalyst, introduction of a little cerium species would be beneficial to the catalytic performance, relating to improved Ni dispersion, metal area and smaller sizes of Ni nanoparticles, the conversion of sorbitol increased with the increasing cerium contents under identical reaction conditions [20]. However, the selectivity to 1,2-PG and EG decreased while more byproducts were formed with higher loading of cerium species owing to excessive hydrogenolysis of intermediate products. The yield of glycols reached to maximum of 36.7% when the M–10Ni2CeAl as catalyst. Therefore, M–10Ni2CeAl was used as a representative in the following studies.

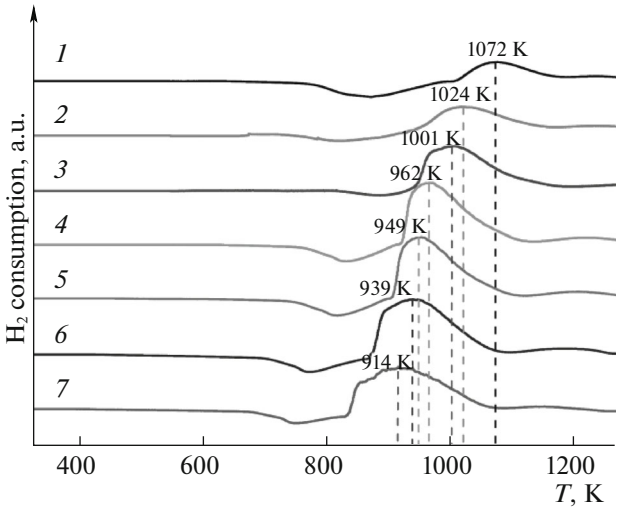

Fig. 3. H_2-TPR profiles for as-calcined catalysts before reduction, (*1*–*7*) see Fig. 1.

Basic promoter plays an important role in the hydrogenolysis of sorbitol, which would accelerate C–C bond cleavage through retro-aldol strategy [12]. Herein, effects of different basic promoters were discussed and the results were listed in Table 3. The conversion of sorbitol increased with the basicity of the selected four hydroxides increasing although the addition amounts of OH^- in those alkaline species were the same. The conversion of sorbitol by the addition of KOH or NaOH was much higher than the results by the addition of $Mg(OH)_2$ and $Ca(OH)_2$, which was attributed to the easier solubility of KOH and NaOH resulting in higher pH values of the solution. However, strong basicity seem to have a negative effect on the selectivity to the glycols by adding KOH and NaOH. With the addition amount of OH^- in the introduced $Ca(OH)_2$ increasing, the conversion of sorbitol would be promoted. Excessive addition amount of $Ca(OH)_2$ would make a drop of glycols selectivity owing to higher basicity. The yield of glycols was as high as 42.3% when the addition amount of $Ca(OH)_2$ was 0.20 g. In addition, in order to investigate the effect of Ca^{2+} in the solution, the $Ca(NO_3)_2$ was selected as promoter and the result was also listed in Table 3.

Table 2. Catalytic performance of different M–*x*Ni*y*CeAl catalysts for sorbitol hydrogenolysis

Catalysts	Sorbitol conversion, %	Selectivity, %						$Y_{glycols}$, %[d]
		glycerol	1,2-PG	EG	C_{4-5}[a]	gas products[b]	others[c]	
None	0.0	–	–	–	–	–	–	–
M-Al_2O_3	0.0	–	–	–	–	–	–	–
M-2CeAl	0.0	–	–	–	–	–	–	–
M-4NiAl	24.6	38.3	30.2	20.7	6.1	1.6	3.1	12.5
M-6NiAl	31.9	36.1	31.9	20.8	3.8	1.9	5.5	16.8
M-8NiAl	36.2	34.5	34.2	22.3	2.5	2.4	4.1	20.5
M-10NiAl	40.8	30.1	37.2	23.9	1.5	3.7	3.6	24.9
M-10Ni1CeAl	54.1	27.4	38.9	22.4	2.1	4.5	4.7	33.2
M-10Ni2CeAl	62.3	25.3	37.7	21.2	1.8	5.6	8.4	36.7
M-10Ni4CeAl	66.5	19.4	34.9	19.1	1.4	12.3	12.9	35.9

Reaction conditions: sorbitol (30 wt % aqueous solution) = 20 mL; catalyst, 0.60 g; $Ca(OH)_2$ 0.10 g; 493 K; time, 8 h; $P(H_2)$, 4.0 MPa.
[a] C_{4-5}: xylitol, erythritol and 1,2-butanediol.
[b] Gas products: CH_4 and CO_2.
[c] Others: lactic acid, ethanol, methanol, 1-propanol and 2-propanol.
[d] $Y_{glycols}$: yield of EG and 1,2-PG.

Table 3. Effect of basic promoter on the hydrogenolysis of sorbitol

Promoter	Amount of promoter, g	Amount of OH^- in promoter, mmol	Sorbitol conversion, %	Selectivity, %						$Y_{glycols}$, %[d]
				glycerol	1,2-PG	EG	C_{4-5}[a]	gas products[b]	others[c]	
–	0.00	0.00	32.1	22.6	21.4	16.6	28.2	1.6	9.6	12.2
KOH	0.08	1.35	88.3	4.8	13.1	8.6	1.8	13.3	58.4	19.2
NaOH	0.05	1.35	83.6	5.1	13.9	10.8	1.6	12.3	56.3	20.6
$Mg(OH)_2$	0.08	1.35	46.8	25.6	36.2	16.4	7.7	3.5	10.6	24.6
$Ca(OH)_2$	0.10	1.35	62.3	25.3	37.7	21.2	1.8	5.6	8.4	36.7
$Ca(OH)_2$	0.20	2.70	71.6	26.6	36.5	22.6	1.3	6.8	6.2	42.3
$Ca(OH)_2$	0.40	5.40	79.3	17.4	23.1	17.9	1.2	16.1	24.3	32.5
$Ca(NO_3)_2$	0.10	0.00	32.8	21.1	20.4	17.1	26.2	1.4	13.8	12.3

Reaction conditions: sorbitol (30 wt % aqueous solution) = 20 mL; catalyst, 0.60 g; 493 K; time, 8 h; $P(H_2)$, 4.0 MPa.
[a] C_{4-5}: xylitol, erythritol and 1,2-butanediol.
[b] Gas products: CH_4 and CO_2.
[c] Others: lactic acid, ethanol, methanol, 1-propanol, and 2-propanol.
[d] $Y_{glycols}$: yield of EG and 1,2-PG.

Although the hydrogenolysis of sorbitol could be promoted by C–C cleavage owing to the formation of Ca^{2+} complexes proposed by Zhou et al. [26] no obvious enhancement could be found in the absence of OH^-.

Reaction temperature is an important factor in the hydrogenolysis of sorbitol, which has a significant effect on catalytic performance. As shown in Fig. 4, the conversion of sorbitol increased rapidly with reaction temperature increasing from 433 to 513 K, whereas the total selectivity of 1,2-PG and EG reached 56.1% at 493 K followed by a significant drop owing to the excessive hydrogenolysis resulting in the increase of the selectivity to gas products. Although the yield of glycols under 513 K was slightly higher, more gas products would be formed, whose commercial value was much lower. Therefore, the appropriate reaction temperature was 493 K.

The influence of variation in H_2 pressure on the reaction was presented in Fig. 5. It could be seen that higher H_2 reaction pressure had a positive effect on the

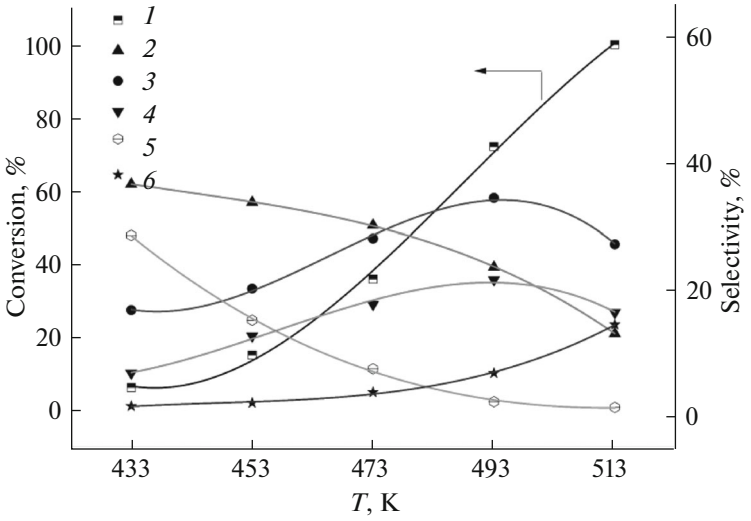

Fig. 4. Effect of reaction temperature on the hydrogenolysis of sorbitol over M–10Ni2CeAl catalyst; (*1*) conversion of sorbitol and selectivity to (*2*) glycerol, (*3*) 1,2-PG, (*4*) EG, (*5*) $C_{4\text{-}5}$, (*6*) gas products. Reaction conditions: sorbitol (30 wt % aqueous solution), 20 mL; catalyst, 0.60 g; $Ca(OH)_2$, 0.20 g; time, 8 h; $P(H_2)$, 4.0 MPa.

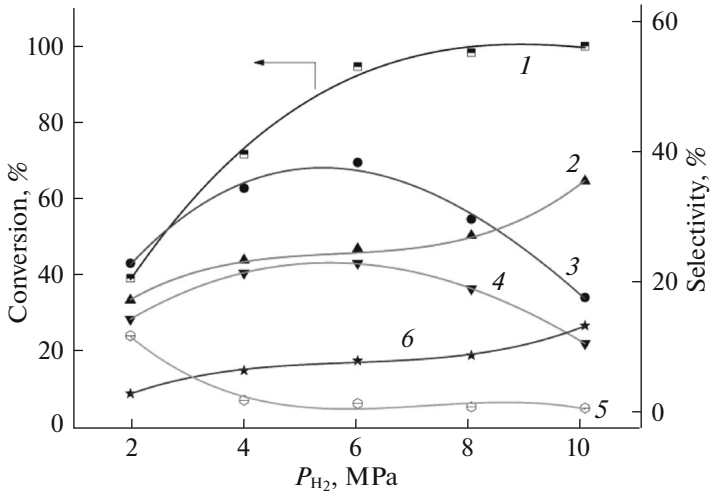

Fig. 5. Effect of H_2 pressure on the hydrogenolysis of sorbitol over M–10Ni2CeAl catalyst. Reaction conditions: sorbitol (30 wt % aqueous solution), 20 mL; catalyst, 0.60 g; $Ca(OH)_2$, 0.20 g; temp., 493 K; time, 8 h; (*1*–*6*) see Fig. 4.

hydrogenolysis of sorbitol because the conversion of sorbitol increased significantly under higher H_2 pressure. Total selectivity of 1,2-PG and EG reached to maximum of 61.5% at 6 MPa, the sorbitol conversion of 94.5% and yield of 1,2-PG and EG as high as 58.1% were obtained and decreased under higher H_2 pressure owing to further degradation. The selectivity to $C_{4\text{-}5}$ polyols almost decreased to around 2% when the H_2 pressure was higher than 4 MPa and the selectivity of glycerol and gas products increased rapidly with the H_2 pressure increasing, suggesting that the excessive hydrogenolysis would be promoted under higher H_2 pressure. The selectivity of EG and 1,2-PG was dropped with the H_2 pressure increasing higher than 6 MPa, which may be owing to further hydrogenolysis of reaction intermediates to lighter products, resulting in more gas components in the final product.

The influence of reaction time on the reaction were presented in Fig. 6. With the increase of reaction time, sorbitol conversion increased gradually until complete hydrogenolysis after 10 h. Considerable amounts of $C_{4\text{-}5}$ polyols and glycerol were obtained when the reaction time was 2 h, while they gradually decreased with reaction time increasing. The yield of 1,2-PG and EG could reach maximum of 58.1% under the reaction time of 8 h, with the further increase of reaction time, it would decrease, which was attributed to their deep

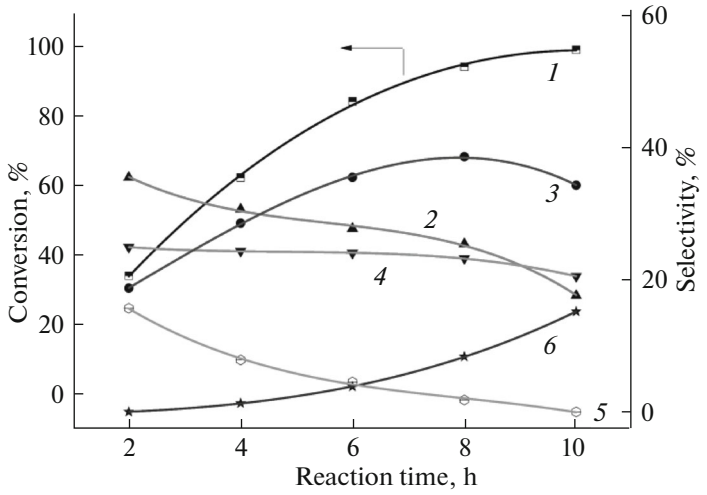

Fig. 6. Effect of reaction time on the hydrogenolysis of sorbitol over M–10Ni2CeAl catalyst Reaction conditions: sorbitol (30 wt % aqueous solution), 20 mL; catalyst, 0.60 g; $Ca(OH)_2$, 0.20 g; temp., 493 K; $P(H_2)$, 6.0 MPa; (*1*–*6*) see Fig. 4.

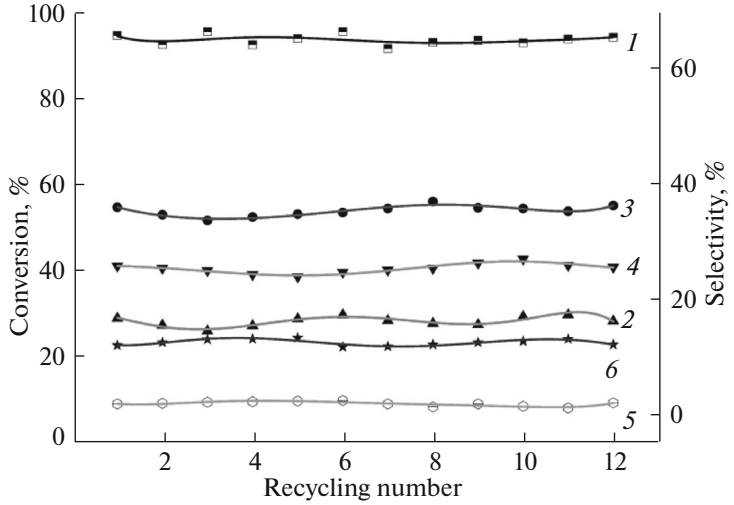

Fig. 7. Catalytic recyclability of M–10Ni2CeAl catalyst for the hydrogenolysis of sorbitol reaction conditions: sorbitol (30 wt % aqueous solution), 20 mL; catalyst, 0.60 g; $Ca(OH)_2$, 0.20 g; temp., 493 K; $P(H_2)$, 6.0 MPa; time, 8 h; (*1*–*6*) see Fig. 4.

degradation resulting in the formation of more lower products.

Endurance Testing

The catalytic stability is very important for the application of a catalyst, so the stability of the M–NiCeAl catalysts was studied in the hydrogenolysis of sorbitol with M–10Ni2CeAl as a representative, and the results were shown in Fig. 7. It could be seen that the catalytic performance maintained steady during 12 runs and the yield of 1,2-PG and EG could maintain to 56.9% after the catalyst being used for 12 cycles, indicating that the as-prepared catalyst had a stable catalytic performance even though it was conducted in the rigorous hydrothermal reaction conditions.

The physical chemical properties of reused M–10Ni2CeAl catalyst after 12 runs denoted as M–10Ni2CeAl–RT were also investigated by different techniques and compared with the results of M–10Ni2CeAl before recycling tests. The XRD diffraction results (see Fig. 1) showed that the peak intensity of Ni nanoparticles slightly increased, and its particle size increased from 6.1 to 6.7 nm based on the Scherer equation. Dispersion measurement revealed the negligible sintering of the Ni nanoparticles, and the ICP results showed that mass fractions of Ni and Ce almost did not change (see Table 1), suggesting no obvious leaching occurred under the condition of alkaline hydrothermal reaction conditions. N_2 adsorption-desorption tests (see Fig. 2) showed that the meso-

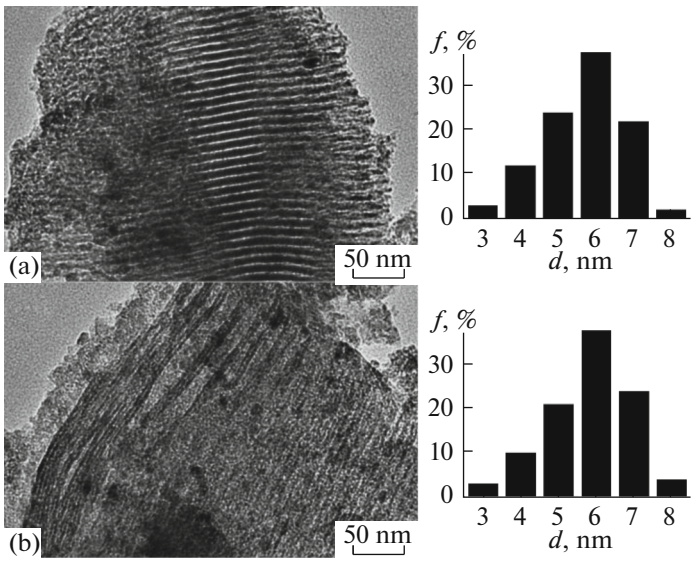

Fig. 8. TEM images and Ni particle size (*d*) distribution for (a) M–10Ni2CeAl and (b) M–10Ni2CeAl–RT catalysts, *f* is frequency.

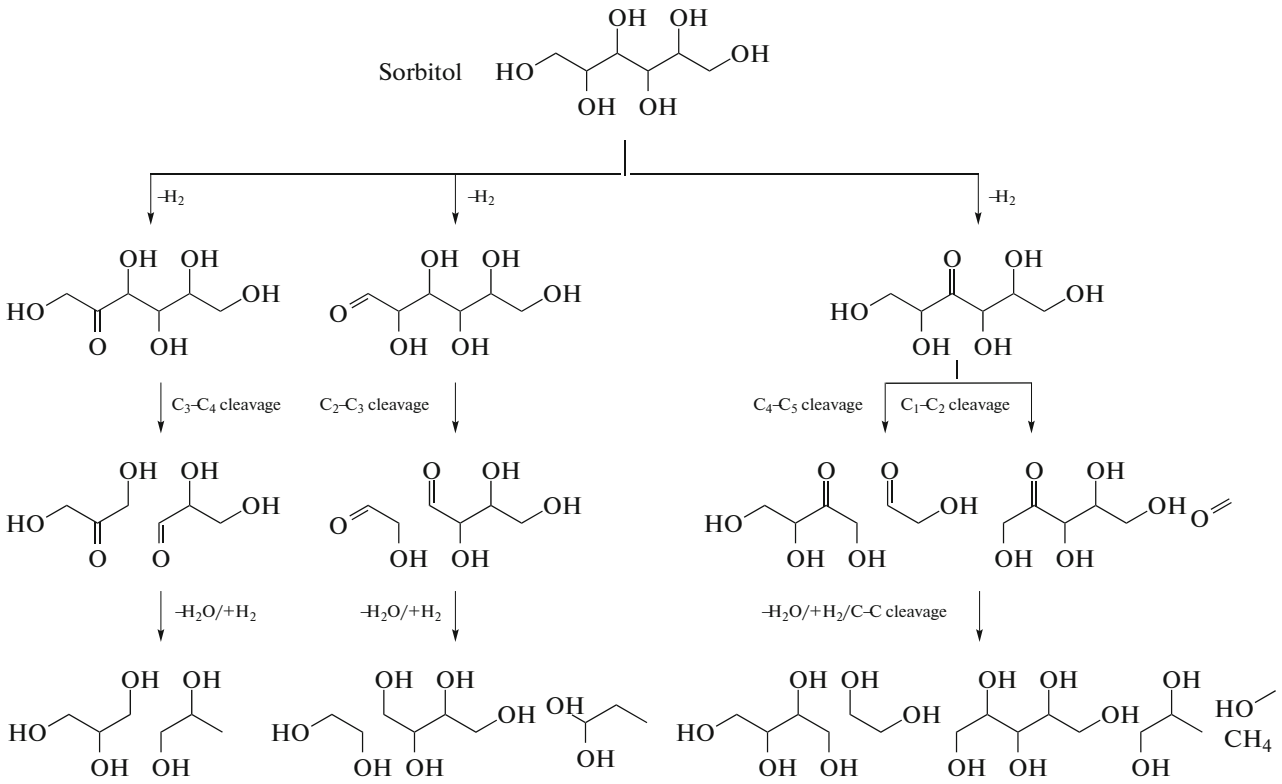

Fig. 9. Possible reaction pathway for the hydrogenolysis of sorbitol over M–NiCeAl catalyst.

porous structure could be maintained and their textural parameters were kept well.

Figure 8 was the TEM images for M–10Ni2CeAl and M–10Ni2CeAl–RT catalysts, and it could be seen that the size distribution of Ni nanoparticles did not change significantly and the mesoporous structure was still maintained, which was coincident with the results of N_2 physisorption. Based on the analysis above, it could be concluded that the as-prepared M–10Ni2CeAl catalyst owned excellent hydrothermal stability and showed good reusability in the hydrogenolysis of sorbitol.

Reaction Mechanism and Reaction Pathway

Based on the analysis above and polyol hydrogenolysis reaction mechanism proposed by Wang et al. [12] detailed possible reaction pathway for the hydrogenolysis of sorbitol was proposed and shown in Fig. 9. Aldehydes or ketones were firstly formed by dehydrogenation of sorbitol adsorbed on the Ni nanoparticles, and then followed by C–C bond cleavage in the presence of OH^- to obtain various intermediates, which could be hydrogenated or dehydroxylated to form products such as 1,2-PG and EG. Simultaneously, they would be transformed to lower products by further hydrogenolysis.

CONCLUSIONS

Ordered mesoporous M–NiCeAl catalysts were designed and prepared by one-pot EISA method and investigated in the hydrogenolysis of sorbitol. The as-prepared samples with narrow pore sizes around 10 nm provided relatively large specific surface areas to homogeneously disperse and embed Ni nanoparticles with sizes about 6 nm into the mesopore channels according to XRD, H_2 impulse chemisorption and TEM results, which would be restrained from sintering and beneficial to the access of sorbitol to active metal sites. Meanwhile, introduction of little cerium species would make the samples easier reduced and lead to improved Ni dispersion, which would be beneficial to its catalytic performance in the hydrogenolysis of sorbitol. The basicity and amount of different basic promoters would significantly affect the catalytic performance, yield of 1,2-PG and EG was the highest when the addition amount of $Ca(OH)_2$ was 0.20 g. The reaction conditions were optimized and the yield to 1,2-PG and EG reached 58.1% over M–10Ni2CeAl catalyst at 493 K under 6 MPa after reaction for 8 h, whose catalytic stability could be kept well after repeated reactions for 12 times in the rigorous hydrothermal reaction conditions. The possible reaction pathway was also proposed. The research results can provide a valuable reference for preparation of catalysts with good catalytic performance and stability for the hydrogenolysis of sorbitol.

ACKNOWLEDGMENTS

This work was supported by Jiangsu Planned Projects for Post-doctoral Research Funds (1302121C); Open Project of Beijing Key Laboratory for Enze Biomass and Fine Chemicals; A Project Funded by the Priority Academic Program Development of Jiangsu Higher Education Institutions (PDAD).

REFERENCES

1. C. H. Zhou, J. N. Beltramini, Y. X. Fan, et al., Chem. Soc. Rev. **37**, 527 (2008).
2. D. M. Alonso, S. G. Wettstein, and J. A. Dumesic, Chem. Soc. Rev. **41**, 8075 (2012).
3. J. N. Chheda, G. W. Huber, and J. A. Dumesic, Angew. Chem. Int. Ed. Engl. **46**, 7164 (2007).
4. R. Rinaldi and F. Schüth, Energ. Environ. Sci. **2**, 610 (2009).
5. C. J. Yue, Q. J. Zhang, L. P. Gu, et al., Asia-Pacif. J. Chem. Eng. **9**, 581 (2014).
6. Y. Li, Y. Liao, X. Cao, et al., Biomass Bioenerg. **74**, 148 (2015).
7. R. Palkovits, K. Tajvidi, J. Procelewska, et al., Green Chem. **12**, 972 (2010).
8. A. M. Ruppert, K. Weinberg, and R. Palkovits, Angew. Chem. Int. Ed. Engl. **51**, 2564 (2012).
9. X. Guo, J. Guan, B. Li, et al., Sci. Rep. **5**, 1 (2015).
10. D. K. Sohounloue, C. Montassier, and J. Barbier, React. Kinet. Catal. Lett. **22**, 391 (1983).
11. I. T. Clark, Ind. Eng. Chem. **50**, 1125 (1958).
12. K. Wang, M. C. Hawley, and T. D. Furney, Ind. Eng. Chem. Res. **34**, 3766 (1995).
13. L. Zhao, J. H. Zhou, Z. J. Sui, et al., Chem. Eng. Sci. **65**, 30 (2010).
14. X. Wang, X. Liu, Y. Xu, et al., Chin. J. Catal. **36**, 1614 (2015).
15. M. Banu, P. Venuvanalingam, R. Shanmugam, et al., Top. Catal. **55**, 897 (2012).
16. W. Du, L. Zheng, J. Shi, et al., Fuel Process Technol. **139**, 86 (2015).
17. W. Du, L. Zheng, X. Li, et al., Appl. Clay Sci. **123**, 166 (2016).
18. X. Chen, X. Wang, S. Yao, et al., Catal. Commun. **39**, 86 (2013).
19. M. Banu, S. Sivasanker, T. M. Sankaranarayanan, et al., Catal. Commun. **12**, 673 (2011).
20. L. Ye, X. Duan, H. Lin, et al., Catal. Today **183**, 65 (2012).
21. S. M. Morris, P. F. Fulvio, and M. Jaroniec, J. Am. Chem. Soc. **130**, 15210 (2008).
22. L. Xu, H. Song, and L. Chou, Catal. Sci. Technol. **1**, 1032 (2011).
23. L. Xu, Z. Miao, H. Song, et al., Int. J. Hydrogen Energ. **39**, 3253 (2014).
24. N. Wang, Z. Xu, J. Deng, et al., ChemCatChem **6**, 1470 (2014).
25. X. Yang, J. Da, H. Yu, et al., Fuel **179**, 353 (2016).
26. J. Zhou, G. Liu, Z. Sui, et al., Chin. J. Catal. **35**, 692 (2014).